HHS Public Access

Author manuscript

Surgery. Author manuscript; available in PMC 2021 July 01.

Published in final edited form as:

Surgery. 2020 July ; 168(1): 85–91. doi:10.1016/j.surg.2020.02.020.

Tumor-specific, near-infrared nanobody probe rapidly labels tumors in an orthotopic mouse model of pancreatic cancer

Thinzar M. Lwin, MD[a], **Sophie Hernot, PhD**[b], **Hannah Hollandsworth, MD**[a,c], **Siamak Amirfakhri, PhD**[a,c], **Filemoni Filemoni**[a,c], **Pieterjan Debie**[b], **Robert M. Hoffman, PhD**[a,c,d], **Michael Bouvet, MD**[a,c,*]

[a]Department of Surgery, University of California San Diego, CA

[b]Laboratory for In vivo Cellular and Molecular Imaging, ICMI-BEFY/MIMA, Vrije Universiteit Brussel, Brussels, Belgium

[c]VA San Diego Healthcare System, CA

[d]AntiCancer, Inc, San Diego, CA

Abstract

Background: Nanobodies, derived from camelid antibodies made of only heavy chains, are the smallest, biologic, antigen-binding fragments (~15kDa) with faster pharmacokinetics and better tumor penetration efficiency than standard antibodies. The present study evaluates the efficacy of a fluorescent, anti-carcinoembryonic antigen nanobody for rapid tumor labeling in an orthotopic mouse model of pancreatic cancer.

Methods: Anti-carcinoembryonic antigen or control nanobodies were conjugated with the near-infrared fluorophore IRDye 800CW. Fragments of BxPC3 or MiaPACA2 human pancreatic cancer cell lines were orthotopically implanted into the pancreatic tail of nude mice. After tumors reached 7 to 10 mm in size, 2 nmol anti-carcinoembryonic antigen or control nanobody-IRDye800CW was injected intravenously. Mice were imaged at various time points hours postinjection.

Results: Carcinoembryonic antigen-expressing, BxPC3 pancreatic orthotopic tumors were fluorescently labeled with aCEA-nb-800 3 hours after injection. The signal was present as early as 15 minutes after injection and was robust at 1 to 3 hours after injection with a tumor-to-background ratio of 2.66. In contrast, there was very low accumulation in the low carcinoembryonic antigen-expressing, MiaPACA2 pancreatic orthotopic tumors. The fluorophore-conjugated nanobody was specific for carcinoembryonic antigen-expressing tumors, while the control nanobody did not show any tumor-specific signal. Both nanobodies had strong kidney uptake as expected for small-molecule probes. The fluorescence signal was detectable using 2

*Reprint requests: Michael Bouvet, MD, University of California, San Diego, Department of Surgery, Moores UCSD Cancer Center, 3855 Health Science Drive #0987, La Jolla, CA 92093-0987. mbouvet@ucsd.edu (M. Bouvet).

Author contributions include study conception and design: TL, SH, ND, MB; probe development: SH, PD; acquisition of data: TL, SA, FF; analysis and interpretation of data: TL, SH, MB; drafting of manuscript: TL, RMH, MB; and critical revision: TL, RMH, MB.

Conflict of interest/Disclosure

The authors have no conflicts of interest to disclose.

Supplementary materials

Supplementary material associated with this article can be found, in the online version, at https://doi.org/10.1016/j.surg.2020.02.020.

clinical, Food and Drug Administration-approved, 800 nm imaging devices as well as small animal imaging systems.

Conclusion: This anti-carcinoembryonic antigen, nanobody-based, fluorescent probe labeled pancreatic orthotopic tumors within 15 minutes of intravenous injection. Fluorescent anti-carcinoembryonic antigen nanobodies have labeling kinetics that approach the speed of nonspecific dyes such as indocyanine green but with the specificity of antibodies. The use of fluorescently-labeled, intact antibodies leads to a labeling delay of 48 to 96 hours between probe administration and the necessarily delayed time of operation, which can be avoided with nanobodies. The kinetics of a nanobody-based probe makes it a practical agent for same-day, patient administration and fluorescence-guided surgery.

TOC summary

This study evaluates the efficacy of a fluorescent, anti-carcinoembryonic antigen nanobody for rapid tumor labeling in an orthotopic mouse model of pancreatic cancer. This study is important, because this anti-carcinoembryonic antigen, nanobody-based, fluorescent probe labeled small pancreatic orthotopic tumors within 15 minutes of intravenous injection, approaching the speed of non-specific dyes, such as indocyanine green, but with the specificity of antibodies.

Background

Complete operative resection of cancer is the goal of all curativeintent oncologic operations. Currently, surgeons rely on visual and tactile cues to distinguish tumors from surrounding tissue, but this technique is inadequate. Positive resection margins are found in up to 84% of patients with pancreatic cancer and 24% of patients with rectal cancer.[1,2] Novel techniques able to rapidly and specifically visualize resection margins in real time are necessary to increase the rate of complete (R0) resections. Navigation with fluorescence guidance has emerged as a promising strategy to improve the precision of oncologic surgery.[3–7] Our lab has pioneered fluorescence-guided surgery (FGS) using orthotopic mouse models of cancers using both genetic reporters and fluorescent antibodies to specifically label the neoplasms.[8–11]

Antibody-linked fluorophores have both reliably and specifically labeled tumors in vivo in both preclinical and clinical settings.[12,13] But the large size of intact antibodies of approximately 150 kilo-Daltons (kDa) leads to decreased efficacy of target penetration, delays in the peak signal, and a long serum half-life.[14] These factors become an important issue in the timing of operation, because there is a substantial delay between administration of an antibody-fluorophore conjugate and timing of the operation.[7] Post-operatively, the antibody-fluorophore conjugate can remain circulating in the serum for an extended period of time.

Engineered antibody fragmentation is a possible solution to this issue, which can retain binding efficacy while decreasing size. Single-chain, variable fragments are small fusion proteins (25 kDa) composed of the variable region of the heavy and light chains of antibodies with improved tumor penetration; however, these single-chain, variable fragments show spontaneous dimerization and decreased affinity.[15] Nanobodies are the next generation

of mini-antibodies derived from camelid heavy chain antibodies.[16] They are single domain, variable fragments of about 15 kDa in size. These molecules retain the affinity of intact antibodies but can penetrate and bind antigens rapidly at sites not easily accessible to larger molecules. Furthermore, nanobodies are more pH-stable, heat-stable, and resistant to proteolytic degradation making them an ideal platform for creating tumor-specific imaging agents.[17]

The present report describes the use of a site-specific, conjugated fluorescent nanobody probe for delivering tumor-specific, near-infrared (NIR) fluorescence in a clinically relevant, orthotopic, xenograft mouse model. Here we show that this construct not only can quickly and effectively target the tumor to deliver fluorescence but also is compatible with existing, Food and Drug Administration (FDA)-approved, NIR fluorescence operative imaging devices to provide contrast for FGS.

Study design

Cell culture—The human pancreatic cancer cell lines BxPC-3 (ATCC CRL-1687; ATCC, Manassas, VA), stably expressing green fluorescent protein (GFP) and MiaPACA-2 (ATCC CRL-1420; ATCC) expressing RFP (red fluorescent protein; AntiCancer Inc, San Diego, CA), were maintained in Roswell Park Memorial Institute 1640 (RPMI-1640) medium (Gibco-BRL, Grand Island, NY). The medium was supplemented with 10% fetal calf serum (Hyclone, Logan, UT), 1% L-Glutamine, and 1% penicillin/streptomycin (Gibco-BRL). The cells were incubated at 37°C in a 5% CO_2 incubator.

Synthesis and conjugation of the nanobody—Previously generated anti-carcinoembryonic antigen (NbCEA5) or control nanobodies (R3B23) were produced as described previously.[18–20] Briefly, the nanobody constructs with a carboxy-terminal cysteine tag were cloned into a pHEN6c plasmid and expressed in *E. coli*. Nanobody products were purified from periplasmic extracts using an immobilized, metal affinity chromatography followed by subsequent size-exclusion chromatography. The purified nanobodies were reduced and incubated subsequently at pH 7 with a 5-fold molar excess of IRDye 800CW Maleimide (LI-COR Biosciences, Lincoln, NE).[21] The fluorescently labeled nanobodies were purified using size-exclusion chromatography. The purified flwere puri-conjugated nanobodies are termed aCEA-nb-800 and aCtrl-nb-800.

Animal care—Immunocompromised, nude, nu/fox mice were maintained in a barrier facility on high-efficiency particulate air-filtered racks (AntiCancer Inc, San Diego, CA). Mice were maintained ad lib on an autoclaved laboratory rodent diet (LM-485; Western Research Products, Orange, CA) and kept on a 12 h light/12 h dark cycle. Four-week-old male or female nude mice were used for tumor implantation. All operative procedures and intravital imaging were performed with the animals anesthetized by intramuscular injection of an anesthetic cocktail composed of ketamine 100 mg/kg (MWI Animal Health, Boise, ID), xylazine 10 mg/kg (VWR, Brisbane, CA), and acepromazine 3 mg/kg (Sigma-Aldrich, Saint Louis, MO). All animal studies were conducted in accordance with the principles and procedures outlined in the National Institutes of Health Guide for the Care and Use of Animals under PHS Assurance Number A3873–1.

Mouse Studies—BxPC-3-GFP pancreatic cancer cells (1×10^6 cells per animal) were injected subcutaneously into the flank of these nude mice. The tumors were allowed to grow for 4 weeks or until 7 to 10 mm in size. The tumors were harvested and minced into 2 mm^3 fragments which were implanted into the pancreatic tail of recipient nude mice to create orthotopic models of pancreatic cancer using the technique of operative orthotopic implantation.[22]

Fluorescence Imaging—After 4 to 6 weeks of orthotopic tumor growth when the tumors were palpable at approximately 7 to 10 mm each, the mice were injected with either aCtrl-nb-800 or aCEA-nb-800. The mice were imaged at specific time intervals (hours) postinjection of fluorescent nanobodies using the following imaging systems: the CRI Maestro small animal imaging system with a tunable filter and spectral separation (Perkin Elmer, Waltham, MA), the Pearl Trilogy small animal imager (LI-COR Biosciences, Lincoln, NE), the daVinci Firefly robotic laparoscope (Intuitive Surgical, Sunnyvale, CA), and the Stryker AIM laparoscope (Stryker Corp, Kalamazoo, MI). Time course imaging was as follows: mouse kidneys were imaged non-invasively at 3, 5, and 15 minutes after injection of aCEA-nb-800. After 15 minutes, mice bearing BxPC3-GFP, orthotopic, pancreatic xenografts ($n = 3$) were anesthetized, and a small mini laparotomy was performed to extract the pancreatic tail bearing the implanted tumor. Mice were sequentially imaged at 15 minutes, 30 minutes, 45 minutes, and then at 1, 2, and 3 hours later. Mice were monitored continually and kept warm and under complete anesthesia for the duration of the procedure. Mice were monitored for muscular tone, response to stimulation, and rate and depth of respiration, and anesthesia was re-dosed appropriately. For tumor-specific imaging, aCEA-nb-800 ($n = 4$) or aCtrl-nb-800 ($n = 2$) was compared in mice bearing BxPC3-GFP orthotopic pancreatic xenografts. To confirm specificity to CEA expression, mice bearing CEA-expressing, BxPC3-GFP, orthotopic pancreatic xenografts ($n = 4$) were compared with mice bearing low CEA-expressing, MiaPACA2-RFP, orthotopic pancreatic xenografts ($n = 2$) using aCEAnb-800. Mice were anesthetized and killed 3 hours after injection, and a full laparotomy and intravital imaging were performed.

Images on the Maestro CRI were acquired at the GFP wavelength (excitation 488 nm, emission 510 nm), RFP wavelength (excitation 558 nm, emission 583 nm), and IRDye 800 wavelength (excitation 778 nm, emission 800 nm). Peak intensity of fluorescence was quantified at regions of interests on the skin, tumor, and kidneys after spectral unmixing using the Maestro CRI software. Units for quantification of fluorescence intensity are arbitrary units per CRI Maestro software. Images on the Pearl Trilogy were acquired at the 800 nm wavelength. Peak fluorescence intensity was quantified at regions of interest on skin, tumor, and kidneys using the built-in Image Studio 4.0 Software. Units for quantification of fluorescence intensity are indicated as arbitrary units per Image Studio 4.0 Software.

Images on the daVinci Firefly were acquired after placing the animal within the robotic simulation dome and switching between the bright light and the Firefly mode. Still images and video clips were acquired using the standard capture software within the robotic imaging tower. Images using the Stryker AIM were acquired using the same robotic

simulation dome with the 5 mm, zero-degree scope. Still images and video clips were acquired using the standard capture software within the laparoscopic imaging tower

Statistics

SPSS Statistics Software version 24.0 (IBM Corp, Armonk, NY) was used for data analysis. A *P* value ≤.05 was considered statistically significant. Tumor-to-background ratio (TBR) was calculated by dividing the peak fluorescence intensity at the tumor by the peak fluorescence intensity at a representative area of overlying skin. Data are reported as mean ± standard deviation. An independent-samples *t* test was performed to compare the peak fluorescence intensity and TBR between groups. Standard error bars are indicated on figures.

Results

The fluorophore-conjugated nanobody specifically co-localized with the GFP-expressing, orthotopic tumor in BxPC3 pancreatic orthotopic xenografts using CEA-nb-800 as indicated by arrows (Fig 1, A–C), while the control nanobody did not show a tumor-specific signal (Fig 1, D–F).

Using aCEA-nb-800 in a MiaPACA2, pancreatic, orthotopic xenograft with low CEA expression, no co-localization of fluorescence signal with the RFP-expressing, orthotopic tumor was observed as indicated by arrows (Fig 2, A–C).

A time course of fluorescence labeling of aCEA-nb-800 in BxPC3 orthotopic xenograft bearing mice is shown in Fig 3. There was a signal present at the tumor as early as 15 minutes after injection. The TBR at 15 minutes was 1.81 ± 0.13. The TBR at other time points was as follows: 30 minutes (1.86 ± 0.14), 45 minutes (2.01 ± 0.21), 1 hour (2.18 ± 0.41), 2 hours (2.32 ± 0.80), and 3 hours (2.20 ± 0.68). There was a rapid uptake of the signal at the skin within 3 to 5 minutes which started to slowly decrease after 15 minutes. There was a rapid uptake of the signal at the kidneys within 15 minutes which plateaued over time.

There was a difference between aCEA-nb-800 and aCtrl-nb-800 in peak fluorescence intensity value at the BxPC3 orthotopic pancreatic tumors 3 hours (1,456.86 ± 573.24 vs 154.18 ± 107.17, P = .0395) (Fig 4, A). There was also a difference in TBR at BxPC3 tumors using aCEA-nb-800 compared with aCtrl-nb-800 at 3 hours (2.66 vs 0.59, P = .0179) (Fig 4, B). The peak fluorescence signal using aCEA-nb-800 was greater in the high-CEA expressing BxPC3 tumors compared with the low-CEA expressing MiaPACA2 tumors (1,456.86 ± 573.24 compared with 229.87± 93.45, P = .047) (Fig 4, C). The TBR using aCEA-nb-800 was also greater in BxPC3 tumors compared with MiaPACA2 tumors (2.66 vs 0.50, P =.0116) (Fig 4, D).

Both aCEA and aCtrl nanobodies had very strong uptake by the kidney observed when the overlying bowel and tumor was mobilized to expose the kidneys directly (Fig 5). The peak fluorescence intensity values at the kidneys were between 4,025 and 4,046, with 4,046 being the maximal threshold of detection by the NIR sensor during data acquisition. The kidneys

are not visualized under the GFP wavelength but fluoresce strongly under the NIR wavelength (Fig 5, A and C). The fluorescence from renal elimination can lead to a stronger signal than that of the fluorescence from tumor-specific binding (Fig 5, B and D). Although there is a very strong renal elimination signal, even BxPC3 pancreatic orthotopic tumors less than 1 cm can be detectable using the aCEA-nb-800. In Supplemental Fig S1, a mini-laparotomy is performed in a mouse with a barely palpable tumor 3 hours after intravenous injection of aCEA-nb-800. The tumor is ~3 mm and the TBR is 2.68 for this image.

Representative images from fluorescence imaging using the Stryker AIM laparoscopic camera are shown in Fig 6. Tumors are approximately 7 mm to 1 cm in diameter at the time of imaging. The set up for fluorescence imaging using the da Vinci Firefly and Stryker AIM laparoscopic cameras is shown in Fig S2. The fluorescence signal was detectable using both of two clinically available, minimally invasive fluorescence imaging systems as shown in attached video clips.

Discussion

The aCEA-nb-800 rapidly and successfully labeled CEA-expressing, BxPC3 pancreatic, orthotopic xenografts in situ within 15 minutes of injection. The probe was specific for the tumor and co-registered with the GFP expressed by the tumor. This was not the case with the aCtrl-nb-800 that showed no specific binding. To confirm that the in vivo nanobody binding was specific to CEA-expressing tumors, the probe was injected into low CEA-expressing MiaPACA-2, orthotopic, xenograft-bearing mice. While there was some tumor localization of the probe, the fluorescence intensity was very low compared with BxPC3 tumors (Figs 1, 2, and 4, A–D). The low level of localization compared with the control nanobody is apparently owing to the low levels of CEA expressed by this cell line that can be seen on fluorescence microscopy.[23]

The TBR of the probe for the BxPC3 CEA-expressing tumors was 2.66 vs 0.59, P = .0179, an adequate signal for a molecule bearing 1 fluorophore per nanobody molecule. Fluorophores have been linked traditionally to antibodies by random conjugation with N-Hydroxysuccinimide ester linkages to primary amines groups.[24] The approach is rapid and effective, but the resulting conjugate is a heterogeneous mixture, with anywhere from 1 to 8 dye molecules attached to varying locations on the antibody. In small molecules such as nanobodies, this approach can hinder the binding to the complementarity determining region. Therefore, site-directed fluorophore linkage was used to label the nanobodies in this experiment, because this approach decreases the heterogeneity of the end product and avoids steric hindrance of the antigen-binding domain leading to improved probe-to-target binding.[21]

Compared to full length antibodies which can carry more fluorophores, a TBR of 2.66 is promising. While this nanobody probe has not yet been evaluated in spontaneous or induced models of pancreatic cancer, an aCEA-antibody-IRDye800CW fluorescent antibody was evaluated in a patient-derived, orthotopic xenograft model of pancreatic cancer, a clinically relevant model with a heterogeneous stroma and spontaneous metastases. The full-length fluorescent antibody probe clearly labeled spontaneously metastasized peritoneal and

abdominal wall implants with a TBR of 3.5.[25] This value is less than cell line-based tumors owing to increased tumor density and decreased antigenic density from stromal elements. Future work is planned to evaluate the pharmacokinetics of aCEA-nb-800 in a patient-derived, orthotopic xenograft model; while fluorescence intensity is expected to decrease owing to stromal contribution in a patient-derived, orthotopic xenograft model, the increased efficiency in penetration in dense tissue by this small molecule could potentially counteract the degree of decrease in fluorescence intensity.

This small nanobody probe had rapid renal accumulation as expected for relatively small molecular probes (Fig 3). The TBR plateaued around 1 to 3 hours and did not interfere with tumor-specific imaging. A very strong, non-specific kidney signal accumulated within 15 minutes, but this signal accumulation was similar to the control nanobody (Figs 4, A and C, and 5). The renal signal can overwhelm that of the tumor-specific binding, which is a critical drawback of these probes and must be taken under consideration. In mice, there is only scant tissue surrounding the kidneys, but in humans, this may be less of an issue as the perinephric fat pad in the retroperitoneum along with Gerota's fascia is more substantial. The kidneys can be shielded from imaging or gently retracted out of the field of inspection if operating directly adjacent to them.

In addition to intraoperative localization to determine resection margins and surveillance of the resection bed to detect residual disease, these agents have the potential to enhance contrast and improve visualization during diagnostic laparoscopy. Radiographically occult peritoneal metastases are seen up to 10% of the time despite the use of high-resolution computed tomography.[26] The probe was able to detect tumors less than 1 cm using the Pearl Trilogy, small animal imager (Fig S1). The use of this technology in fluorescence-guided diagnostic laparoscopy may help avoid laparotomy for cases not amenable to curative resection.

The rapid labeling kinetics of nanobodies is beneficial for FGS on the same day of probe injection, especially when compared with fluorescent probes constructed from full length antibodies. Patients are required to make a separate visit for infusion and postinfusion monitoring which adds cost and effort. This agent can be given in the preoperative holding area or at various points intraoperatively depending on the surgeon preference. The patients are monitored as part of their routine operative course. A tumor-specific signal can even be seen within 15 minutes (Fig 3). In preliminary clinical trials, the anti-HER2 nanobody bound to Gallium-68 showed rapid clearance with an optimal signal-to-noise visualization at 90 minutes without any adverse reaction.[27]

Repeated dosing of the agent has not been studied, but it is unclear what effect this will have on the tumor-specific signal as well as the sensitivity and specificity of the probe. There is no consensus on the minimal threshold of tumor burden needed for FGS. While traditionally, a 1 cm^3 tumor with at least 1×10^9 cells has generally been the amount of tumor that is clinically detectable with bright light visualization with the naked eye.[28] Using contrast enhancement from tumor-specific fluorescence, this number may be as low as 2.4×10^4 in cells with high target expression.[29] It is unclear if there is a dose-dependent effect

proportional to tumor burden or changes in fluorescence signal after neoadjuvant therapies. It is an area that can be investigated in subsequent studies.

The present work demonstrates the feasibility of fluorescent nanobodies as a platform for tumor-specific imaging for pancreatic cancer. In addition to CEA, other antigens overexpressed in cancers can potentially be targeted individually or in combination. Our laboratory program has evaluated other markers such as CA19–9, and the Rosenthal lab is developing a body of work targeting cetuximab for FGS of pancreatic cancer.[30,31] Hernot's group has previous evaluated an anti-HER2 nanobody for FGS.[32]

The aCEA-nb-800 is a promising probe with feasibility for use in conjunction with routine FDA-approved 800 nm NIR fluorescence imaging devices, such as the da Vinci Firefly and the Stryker AIM. A number of operating rooms already have this technology in place for indocyanine green imaging. The use of spectral overlap between indocyanine green and IRDye 800CW avoids the need to purchase additional costly imaging devices for tumor-specific fluorescence imaging. The Stryker AIM laparoscope can produce a brighter signal on-screen compared with the da Vinci Firefly, despite the Firefly having a stronger laser light source. The Stryker AIM uses an LED light source and allows the surgeon the option to increase the gain at the push of a button. The brighter fluorescence signal comes at the cost of increased background noise. These characteristics allow the user to optimize the signal to desired preferences at that specific point during the operation. Intuitive Surgical (Sunnyvale, CA) is in the process of developing a second generation of the Firefly camera with increased sensitivity. The current work was not designed to systematically compare the images produced and devices directly. While probe design plays a role, the present work highlights the importance of diagnostic capabilities and sensitivities of each imaging system. The resulting images are variable and unique to each device. These differences appear to be owing to the strength of the light source (laser, LED, versus xenon) or the sensitivities of the camera sensor as well as the processing software as exemplified by the unique in the 2 diagnostic imaging systems demonstrated here. This type of work will be forthcoming as more tumor-specific probes and devices enter clinical trials. There is a need for effective, real-time fluorescence quantification software to facilitate this evaluation.

In conclusion, nanobody-based probes conjugated to NIR-fluorophores rapidly and successfully targeted CEA-expressing orthotopic pancreatic xenografts in nude mice. The probe was specific to CEA and produced a strong tumor-specific signal with an adequate tumor-to-background ratio of 2.66. The rapid labeling kinetics make this an imminently practical agent for same day administration and FGS. The anti-CEA-IRDye800 probe is compatible with FDA-approved, 800 nm fluorescence imaging devices as well as a small animal imaging system. The anti-CEA-IRDye800 probe is a promising molecule for FGS of pancreatic cancer.

Supplementary Material

Refer to Web version on PubMed Central for supplementary material.

Funding/Support

This work was supported by grants CA109949 and CA132971 from the National Cancer Institute (to M.B. and AntiCancer, Inc), Veterans Administration Merit Review Veterans Administration Merit Review Grant number 1 I01 BX003856-01A1 (MB), NIH/NCI T32CA121938 (TL), and P30 2P30CA023100-28 (University of California San Diego Cancer Center Microscopy).

References

1. Ethun CG, Kooby DA. The importance of surgical margins in pancreatic cancer. J Surg Oncol. 2016;113:283–288. [PubMed: 26603829]
2. Pawlik TM, Scoggins CR, Zorzi D, et al. Effect of surgical margin status on survival and site of recurrence after hepatic resection for colorectal metastases. Ann Surg. 2005;241:715–724. [PubMed: 15849507]
3. Bouvet M, Hoffman RM. Toward curative fluorescence-guided surgery of pancreatic cancer. Hepatogastroenterology. 2015;62:715–722. [PubMed: 26897960]
4. DeLong JC, Hoffman RM, Bouvet M. Current status and future perspectives of fluorescence-guided surgery for cancer. Expert Rev Anticancer Ther. 2016;16: 71–81. [PubMed: 26567611]
5. de Boer E, Harlaar NJ, Taruttis A, et al. Optical innovations in surgery. Br J Surg. 2015;102:e56–72. [PubMed: 25627136]
6. Gibbs SL. Near infrared fluorescence for image-guided surgery. Quant Imaging Med Surg. 2012;2:177–187. [PubMed: 23256079]
7. Rosenthal EL, Warram JM, de Boer E, et al. Successful translation of fluorescence navigation during oncologic surgery: a consensus report. J Nucl Med. 2016;57: 144–150. [PubMed: 26449839]
8. Tran Cao HS, Kaushal S, Metildi CA, et al. Tumor-specific fluorescent antibody imaging enables accurate staging laparoscopy in an orthotopic model of pancreatic cancer. Hepatogastroenterology. 2012;59:1994–1999. [PubMed: 22369743]
9. Metildi CA, Kaushal S, Pu M, et al. Fluorescence-guided surgery with a fluorophore-conjugated antibody to carcinoembryonic antigen (CEA), that highlights the tumor, improves surgical resection and increases survival in orthotopic mouse models of human pancreatic cancer. Ann Surg Oncol. 2014;21:1405–1411. [PubMed: 24499827]
10. Metildi CA, Kaushal S, Hardamon CR, et al. Fluorescence-guided surgery allows for more complete resection of pancreatic cancer resulting in longer disease-free survival compared to standard surgery in orthotopic mouse models. J Am Coll Surg. 2012;215:126–135. [PubMed: 22632917]
11. Yano S, Hiroshima Y, Maawy A, et al. Color-coding cancer and stromal cells with genetic reporters in a patient-derived orthotopic xenograft (PDOX) model of pancreatic cancer enhances fluorescence-guided surgery. Cancer Gene Ther. 2015;22:344–350. [PubMed: 26088297]
12. Chi C, Du Y, Ye J, et al. Intraoperative imaging-guided cancer surgery: from current fluorescence molecular imaging methods to future multi-modality imaging technology. Theranostics. 2014;4:1072–1084. [PubMed: 25250092]
13. Lwin TM, Hoffman RM, Bouvet M. The development of fluorescence guided surgery for pancreatic cancer: from bench to clinic. Expert Rev Anticancer Ther. 2018;18:651–662. [PubMed: 29768067]
14. Wu AM. Engineered antibodies for molecular imaging of cancer. Methods. 2014;65:139–147. [PubMed: 24091005]
15. Mabry R, Snavely M. Therapeutic bispecific antibodies: the selection of stable single-chain fragments to overcome engineering obstacles. IDrugs. 2010;13: 543–549. [PubMed: 20721825]
16. Krah S, Schröter C, Zielonka S, Empting M, Valldorf B, Kolmar H. Single-domain antibodies for biomedical applications. Immunopharmacol Immunotoxicol. 2016;38:21–28. [PubMed: 26551147]
17. Cortez-Retamozo V, Backmann N, Senter PD, et al. Efficient cancer therapy with a nanobody-based conjugate. Cancer Res. 2004;64:2853–2857. [PubMed: 15087403]

18. Vaneycken I, Govaert J, Vincke C, et al. In vitro analysis and in vivo tumor targeting of a humanized, grafted nanobody in mice using pinhole SPECT/micro-CT. J Nucl Med. 2010;51:1099–1106. [PubMed: 20554727]
19. Massa S, Xavier C, De Vos J, et al. Site-specific labeling of cysteine-tagged camelid single-domain antibody-fragments for use in molecular imaging. Bioconjug Chem. 2014;25:979–988. [PubMed: 24815083]
20. Lemaire M, D'Huyvetter M, Lahoutte T, et al. Imaging and radioimmunotherapy of multiple myeloma with anti-idiotypic Nanobodies. Leukemia. 2014;28: 444–447. [PubMed: 24166214]
21. Debie P, Van Quathem J, Hansen I, et al. Effect of dye and conjugation chemistry on the biodistribution profile of near-infrared-labeled nanobodies as tracers for image-guided surgery. Mol Pharm. 2017;14:1145–1153. [PubMed: 28245129]
22. Fu X, Guadagni F, Hoffman RM. A metastatic nude-mouse model of human pancreatic cancer constructed orthotopically with histologically intact patient specimens. Proc Natl Acad Sci U S A. 1992;89:5645–5649. [PubMed: 1608975]
23. Lwin TM, Murakami T, Miyake K, et al. Tumor-specific labeling of pancreatic cancer using a humanized anti-CEA antibody conjugated to a near-infrared fluorophore. Ann Surg Oncol. 2018;25:1079–1085. [PubMed: 29372363]
24. Strop P, Liu S-H, Dorywalska M, et al. Location matters: site of conjugation modulates stability and pharmacokinetics of antibody drug conjugates. Chem Biol. 2013;20:161–167. [PubMed: 23438745]
25. Lwin TM, Miyake K, Murakami T, et al. Fluorescent humanized anti-CEA antibody specifically labels metastatic pancreatic cancer in a patient-derived orthotopic xenograft (PDOX) mouse model. Oncotarget. 2018;9:37333–37342. [PubMed: 30647873]
26. Schnelldorfer T, Gagnon AI, Birkett RT, Reynolds G, Murphy KM, Jenkins RL. Staging laparoscopy in pancreatic cancer: a potential role for advanced laparoscopic techniques. J Am Coll Surg. 2014;218:1201–1206. [PubMed: 24698487]
27. Keyaerts M, Xavier C, Heemskerk J, et al. Phase I study of 68Ga-HER2-Nanobody for PET/CT assessment of HER2 expression in breast carcinoma. J Nucl Med. 2016;57:27–33. [PubMed: 26449837]
28. Del Monte U. Does the cell number 10(9) still really fit one gram of tumor tissue? Cell Cycle. 2009;8:505–506. [PubMed: 19176997]
29. Prince AC, Jani A, Korb M, et al. Characterizing the detection threshold for optical imaging in surgical oncology. J Surg Oncol. 2017;116:898–906. [PubMed: 28628728]
30. McElroy M, Kaushal S, Luiken GA, et al. Imaging of primary and metastatic pancreatic cancer using a fluorophore-conjugated anti-CA19–9 antibody for surgical navigation. World J Surg. 2008;32:1057–1066. [PubMed: 18264829]
31. Tummers WS, Miller SE, Teraphongphom NT, et al. Intraoperative pancreatic cancer detection using tumor-specific multimodality molecular imaging. Ann Surg Oncol. 2018;25:1880–1888. [PubMed: 29667116]
32. Debie P, Vanhoeij M, Poortmans N, et al. Improved debulking of peritoneal tumor implants by near-infrared fluorescent nanobody image guidance in an experimental mouse model. Mol Imaging Biol. 2017;20:361–367.

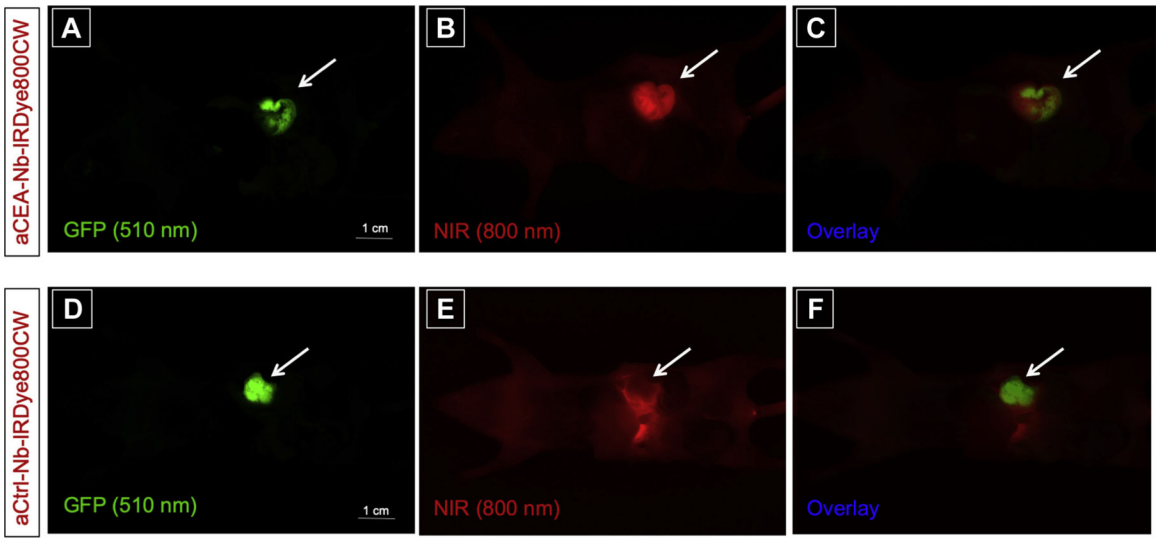

Fig 1.

Anti-CEA nanobody LI-COR-IR800 compared with anti-Control-IRDye800CW nanobody in a BxPC3 pancreatic orthotopic mouse model shows that aCEA-nb-800 nanobody labels BxPC3 pancreatic orthotopic xenografts effectively compared with aCtrl-nb-800. The aCEA-cnb-800 was visualized at the tumor within 3 hours of injection and co-localized with the GFP-tagged orthotopic tumor indicated by arrows (*A*–*C*). The control nanobody did not show a fluorescence signal at the GFP-tagged tumor (*D*–*F*). Scale bar indicates 1 cm. Images were acquired using the CRI Maestro (Caliper Life Sciences, Hopkinton, MA) small animal imager.

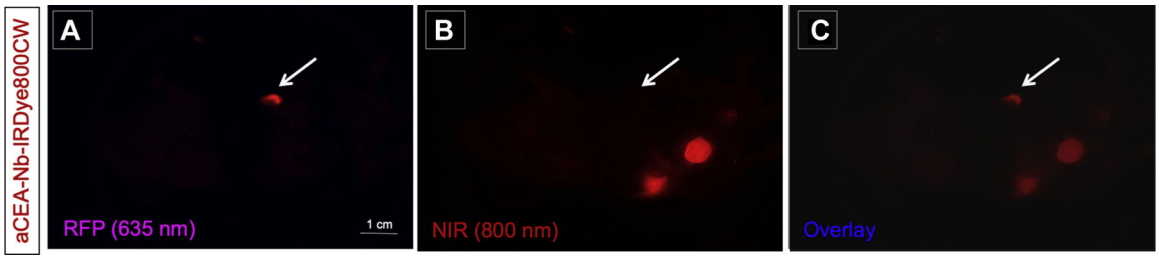

Fig 2.

Anti-CEA nanobody LI-COR-IR800 in a MiaPACA2 pancreatic orthotopic mouse model shows that aCEA-nb-800 nanobody does not effectively label orthotopic MiaPACA2 pancreatic xenograft indicated by arrows (*B*). There is minimal co-localization of 800 nm fluorescence with the RFP-tagged tumor (*A*–*C*). Scale bar indicates 1 cm. Images were acquired using the CRI Maestro small animal imager.

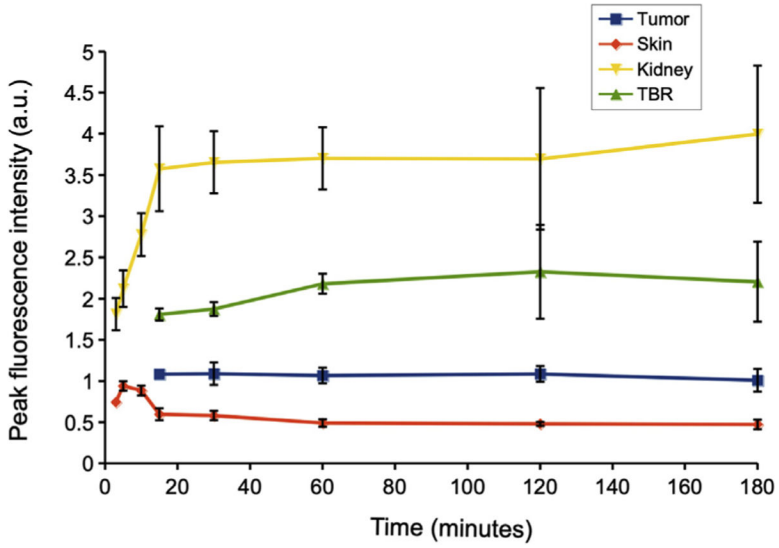

Fig 3.

A time course evaluation of aCEA-nb-800 in BxPC3 orthotopic xenograft bearing mice at different time intervals. There was a signal present at the tumor as early as 15 minutes after injection. The TBR at 15 minutes was 1.81 ± 0.13. The TBR at other time points was as follows: 30 minutes (1.86 ± 0.14), 45 minutes (2.01 ±0.21), 1 hour (2.18 ± 0.41), 2 hours (2.32 ± 0.80), 3 hours (2.20 ±0.68). There was a rapid uptake of the signal at the skin within 3 to 5 minutes which slowly started decreasing after 15 minutes. There was a rapid uptake of the signal at the kidneys within 15 minutes which plateaued over time. Images were acquired using the Pearl Trilogy small animal imager.

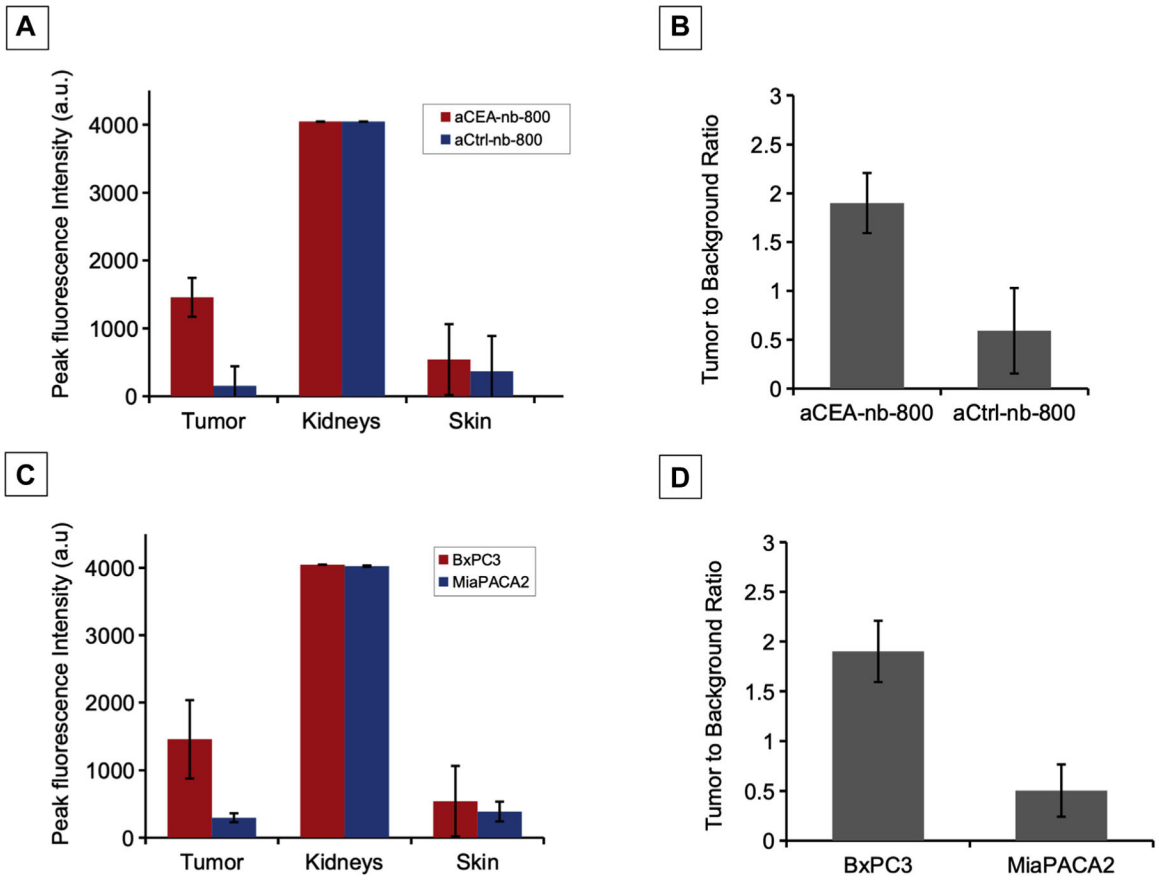

Fig 4.

Quantification of fluorescence signal and calculation of TBR in mouse models using aCEA-nb-800 versus aCtrl-nb-800. The peak fluorescence intensity value at the BxPC3 tumor using aCEA-nb-800 was greater compared with aCtrl-nb-800 was 1,456.86 ± 573.24 vs 154.18 ± 107.17, P = .0395 (*A*). The TBR at the BxPC3 tumor using aCEA-nb-800 was greater compared with the aCtrl-nb-800 at 2.66 vs 0.59, P = .0179 (*B*). The peak fluorescence signal using aCEA-nb-800 was greater in BxPC3 (high-CEA expressing) tumors compared with MiaPACA2 (low-CEA expressing) tumors (1,456.86 ± 573.24 vs 229.87± 93.45, P = .047) (*C*). The TBR using aCEA-nb-800 was also greater in BxPC3 tumors compared with MiaPACA2 tumors (2.66 vs 0.50, P = .0116) (*D*). Fluorescence intensity was quanti fied using the Maestro CRI software.

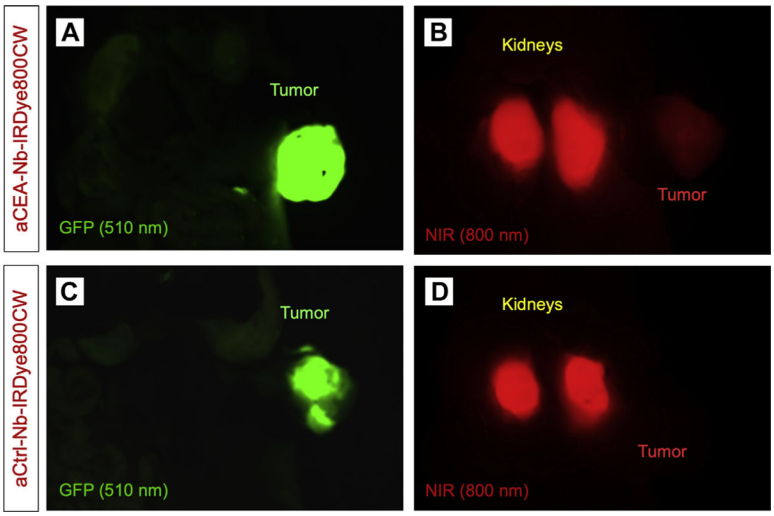

Fig 5.

aCEA and aCtrl nanobodies had very strong kidney signals when the overlying bowel and tumor was mobilized to expose the kidneys directly. They kidneys are not visualized under the GFP wavelength but fluoresce strongly under the NIR wavelength (*A* and *C*). The fluorescence from renal elimination can lead to a stronger signal than that of the fluorescence from tumor-specific binding (*B* and *D*).

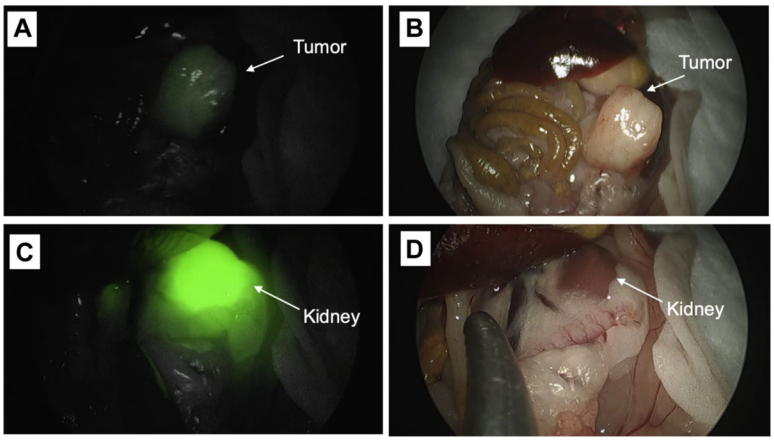

Fig 6.

Representative images from fluorescence imaging using the Stryker AIM laparoscopic camera is shown. Tumors are approximately 7 mm to 1 cm at the time of imaging. The fluorescence signal was detectable using the da Vinci Firefly and Stryker AIM imaging systems as shown in attached video clips.